

Indium incorporation and optical properties of polar, semipolar and nonpolar InAlN

Duc V. Dinh,^{1, a)} Nan Hu,² Yoshio Honda,¹ Hiroshi Amano,^{1,3} and Markus Pristovsek¹

¹⁾*Institute of Materials and Systems for Sustainability, Nagoya University, Nagoya 464-8601, Japan*

²⁾*School of Engineering, Nagoya University, Nagoya 464-8603, Japan*

³⁾*Akasaki Research Center, Nagoya University, Nagoya 464-8603, Japan*

Growth of $\text{In}_x\text{Al}_{1-x}\text{N}$ layers ($0 \leq x \leq 0.45$) by metal-organic vapour phase epitaxy has been investigated simultaneously on polar (0001), untwinned semipolar (10 $\bar{1}$ 3) and nonpolar (10 $\bar{1}$ 0) AlN templates, which were prepared on planar sapphire substrates. The InN mole fraction (x_{InN}) of the layers was tuned by changing growth temperature from 660°C to 860°C. x_{InN} determined by x-ray diffraction was found to be comparable for the polar, semipolar and nonpolar surface orientations. This is consistent with comparable effective bandgap energy of the layers obtained from optical transmission measurements at room-temperature. The bandgap bowing parameter was found to be strongly composition-dependent. Room-temperature photoluminescence measurements showed impurity transitions for the layers with $x_{\text{InN}} \leq 0.2$, while InAlN near-band-edge luminescence was observed for the layers with higher x_{InN} .

I. INTRODUCTION

During the past decades, group III-nitride semiconductors (AlN, GaN, and InN) have attracted much interest because of their applications for light-emitting diodes (LEDs), as well as for high-power and high-frequency electronics. In term of room-temperature bandgap energy (E_g) ranging from $E_g^{\text{InN}} = 0.65 \text{ eV}^1$ to $E_g^{\text{AlN}} = 6.2 \text{ eV}^2$, $\text{In}_x\text{Al}_{1-x}\text{N}$ ($0 \leq x \leq 1$) should possibly be a good candidate for both ultra-violet (UV) and visible LEDs. However, growth and properties of high-quality InAlN alloys are relatively poorly understood as its growth requires drastically different growth conditions due to the large difference in the lattice parameters, bond length, and thermal stability of AlN and InN³. Therefore, for near-UV and visible LEDs operating at above 365 nm, InGaN quantum wells (QWs) have mainly been used as the active regions^{4,5}. For UV LEDs operating at below 365 nm, most groups have been using either AlGaIn QWs⁶ or InAlGaIn QWs with very small percentage of In, e.g., less than 5%⁷. Even though, several groups report high internal quantum efficiency obtained from InAlN materials, which were estimated either by photoluminescence⁸ or cathodoluminescence⁹ under low excitation conditions, an InAlN/AlGaIn-based LED operating at 340 - 350 nm has only recently been reported¹⁰.

Growth on semipolar and nonpolar planes results in a reduction of built-in fields¹¹, which can increase the radiative recombination efficiency of QWs, as already confirmed for InGaIn-based LEDs^{4,12}. However, similar to semipolar¹³⁻¹⁹ and nonpolar AlGaIn^{18,20-22}, a few studies have been performed for semipolar (11 $\bar{2}$ 2) InAlN grown on UV-transparent (11 $\bar{2}$ 2) AlN/sapphire templates^{23,24}. One of the reasons is the limit of available non-*c*-plane AlN substrates^{13,17,21} and templates^{25,26}. Additionally, non-*c*-plane InAlN layers were grown on

quasi-UV-transparent templates and substrates, e.g., semipolar (10 $\bar{1}$ 3) InAlN on (113) yttria-stabilized cubic zirconia substrates²⁷, nonpolar (10 $\bar{1}$ 0) *m*-plane InAlN on *m*-plane GaN substrates⁹ and *m*-plane ZnO substrates^{28,29}, as well as nonpolar (11 $\bar{2}$ 0) *a*-plane InAlN on GaN/sapphire templates³⁰. Among these investigated surface orientations, compositional study has only been done for (0001) vs. (10 $\bar{1}$ 0) InAlN layers⁹ and (0001) vs. (11 $\bar{2}$ 2) InAlN layers²⁴. From these studies, no remarkable difference of the InN mole fraction (x_{InN}) has been found for the layers with different surface orientations.

In this paper, we report on indium incorporation and optical properties of InAlN layers grown simultaneously on polar (0001), untwinned semipolar (10 $\bar{1}$ 3) and nonpolar (10 $\bar{1}$ 0) AlN templates by metal-organic vapour phase epitaxy (MOVPE). Compositional study of these layers has been investigated by x-ray diffraction and room-temperature optical transmission measurements.

II. EXPERIMENTAL

Growth was performed in an EpiQuest 3 × 2-in. close-coupled showerhead MOVPE reactor. Ammonia (NH₃), trimethylindium (TMIn) and trimethylaluminum (TMAI) were used as precursors. To prevent residual gallium that may strongly auto-incorporate in InAlN³¹⁻³³, prior to InAlN epitaxy, the showerhead and chamber inner wall were cleaned to remove residual materials deposited from previous growth experiments. Afterwards, the chamber and susceptor were long-baked at 1300°C, and then coated with about 2- μm -thick AlN layer at the same temperature.

Differently surface-oriented AlN templates grown on sapphire substrates were used to grow InAlN, including (0001) AlN on *c*-plane sapphire, (10 $\bar{1}$ 0) AlN and (10 $\bar{1}$ 3) AlN on *m*-plane sapphire. Growth parameters of the (10 $\bar{1}$ 0) templates are reported elsewhere²⁶. To pro-

^{a)}Electronic mail: duc.vn.dinh@gmail.com

duce untwinned Al-polar (10 $\bar{1}$ 3) AlN templates, about 10-nm-thick (10 $\bar{1}$ 3) AlN layer was initially sputtered onto 2-inch *m*-plane sapphire wafers using directional sputtering^{19,34}. Afterwards, these wafers were loaded into the reactor chamber to grow a 300-nm-thick AlN layer at a surface temperature of 1290°C.

Prior undoped InAlN growth, under a reactor pressure of 2.7 kPa in hydrogen ambient, three differently oriented AlN templates were heated to 1290°C to grow a 100-nm-thick AlN layer with $P_{\text{NH}_3} = 6.2$ Pa and $P_{\text{TMAI}} = 0.16$ Pa. Afterwards, the reactor temperature was reduced to 660–860°C to grow uncapped InAlN layers with a nominal thickness of 120 nm at a pressure of 10 kPa in nitrogen ambient. This corresponds to a growth rate of ~ 0.05 nm/s. During InAlN growth, $P_{\text{TMAI}} = 0.12$ Pa, $P_{\text{TMIIn}} = 0.12$ Pa and $P_{\text{NH}_3} = 1000$ Pa were used. This corresponds to an In/(In+Al) ratio of 0.5 in gas phase and a V/III of ≈ 4100 .

The crystal orientation and structural properties of the (0001), (10 $\bar{1}$ 3) and (10 $\bar{1}$ 0) InAlN samples were characterized using a Malvern Panalytical Empyrean triple-axis high-resolution X-ray diffraction (HR-XRD) system with a $\text{CuK}_{\alpha 1}$ source ($\lambda = 1.5406$ Å). Optical transmission measurements of the samples were performed at room temperature (RT) using a Shimadzu UV-2700 UV-Vis spectrometer. For room-temperature photoluminescence (RT-PL) measurements, the samples were excited by two different excitation sources, including a Krypton Fluoride (KrF) excimer (pulsed) laser (ExciStar XS-200) with excitation energy $E_{\text{ex}} = 5$ eV and an excitation power density (P_{ex}) of 5.6 kW/cm², as well as a He-Cd continuous-wave (cw-)laser with $E_{\text{ex}} = 3.8$ eV and $P_{\text{ex}} = 0.05$ kW/cm².

III. RESULTS AND DISCUSSION

A. Phase purity and composition determination

1. Phase purity

Fig. 1 shows wide-range symmetric 2θ - ω XRD scans of four uncapped InAlN layers grown at 660°C and 860°C on *m*-plane AlN and (10 $\bar{1}$ 3) AlN templates. Besides the (30 $\bar{3}$ 0) diffraction peak of *m*-plane sapphire at $\approx 68.2^\circ$, there are only peaks related to (10 $\bar{1}$ 0) InAlN/AlN (Fig. 1(a)) and (10 $\bar{1}$ 3) InAlN/AlN (Fig. 1(b)). This indicates that these layers are indeed single phase. The InAlN peaks clearly appear in the scans of the layers grown at 660°C, while they are almost unobservable for the layers grown at 860°C. This indicates a higher x_{InN} of the layers grown at 660°C. Additionally, positions of six selected diffraction peaks of metallic indium are marked as asterisk symbols (*) in Fig. 1(b), indicating that there is no metallic inclusion in these layers grown at the employed temperatures.

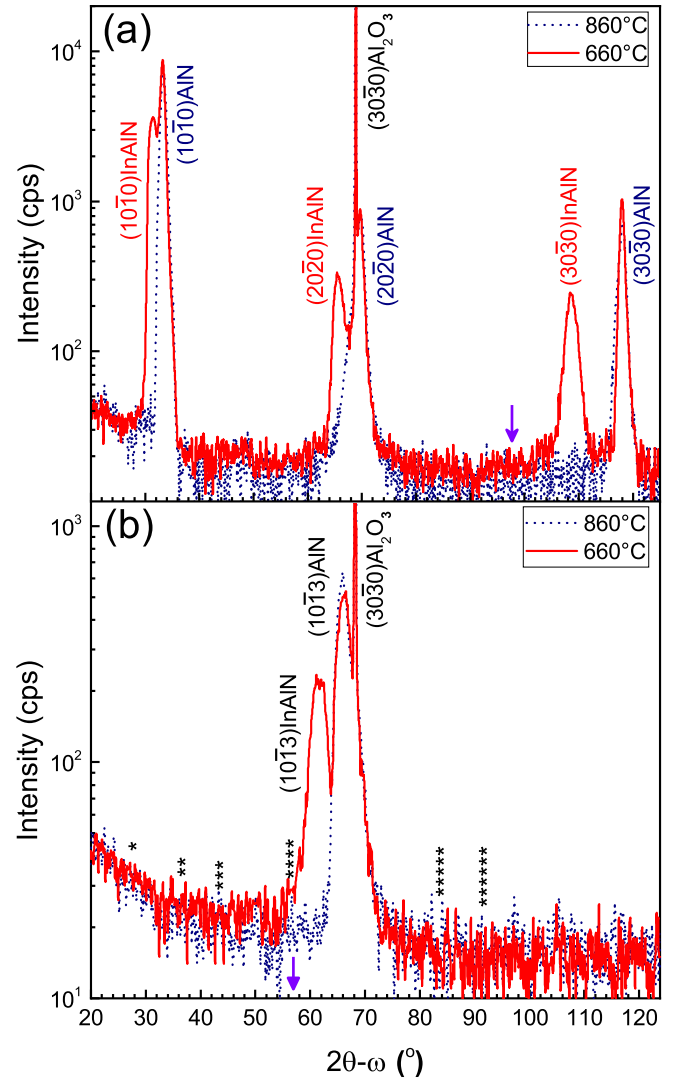


FIG. 1. Symmetric 2θ - ω XRD scans of uncapped InAlN layers simultaneously grown on (10 $\bar{1}$ 0) AlN (a) and (10 $\bar{1}$ 3) AlN templates (b) at different temperatures. These scans were performed with an open detector without any receiving slit. Positions of six selected diffraction peaks of metallic In are marked as asterisk symbols (*) such as (100), (002), (111), (112), (203) and (301) In with increasing 2θ angles. The arrows in (a) and (b) indicate positions of the (30 $\bar{3}$ 0) InN ($\approx 98^\circ$) and (10 $\bar{1}$ 3) InN ($\approx 57^\circ$) diffraction peaks, respectively.

2. Composition determination

Similar to works previously reported for *c*-plane, *m*-plane and untwinned (10 $\bar{1}$ 3) AlGaIn layers^{18,19,22}, for the differently oriented InAlN layers studied here, their x_{InN} were also calculated from high-resolution 2θ - ω measurements of different symmetric, skew-symmetric and asymmetric InAlN diffraction peaks. Fig. 2 shows the calculated x_{InN} as a function of growth temperature. Similar to previously findings for InAlN^{23,24} and InGaIn^{35,36}, x_{InN} of the grown InAlN layers gradually increases with

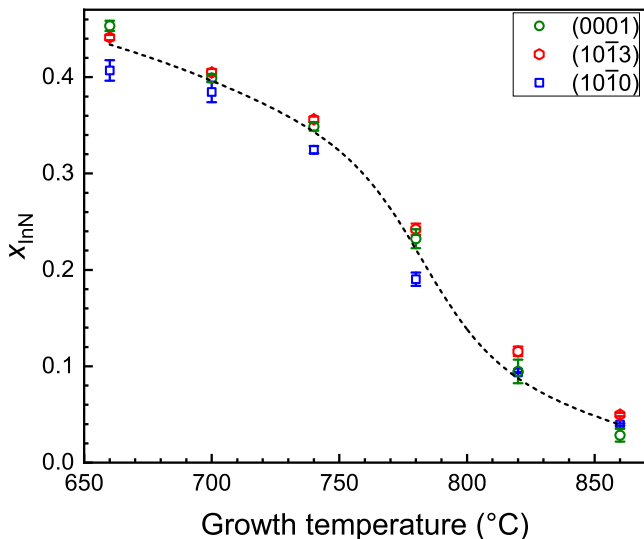


FIG. 2. XRD-calculated x_{InN} of the differently oriented $\text{In}_x\text{Al}_{1-x}\text{N}$ layers as a function of temperature.

decreasing growth temperature, mainly due to the suppression of InN desorption. At each growth temperature, x_{InN} values of the differently oriented layers are quite comparable with x_{InN} of the m -plane layers is little bit lower than the others. A maximum difference of x_{InN} is of less than 0.05 for the layers grown at 660°C and 780°C, while it is smaller than 0.03 for the layers grown at the other temperatures.

In general, different research groups employ different growth conditions (e.g., temperature, pressure and V/III ratio) to grow ternary alloys using MOVPE systems. This might result in different material incorporations on different surface orientations. For example, different results of indium incorporation in c -plane and m -plane InGaN/GaN have previously been reported, e.g., $c < m$ ^{35,49} or $c \approx m$ ³⁶. So far, there is only one report about compositional study of (10 $\bar{1}$ 3) InGaN/GaN, showing that this orientation has the lowest indium incorporation among twenty-five different orientations investigated in Ref. 49. However, indium incorporation in InGaN is mostly limited by desorption, which strongly depends on the surface termination and growth efficiency.

For MOVPE-grown AlGaIn/AlN, it has recently been reported that aluminium incorporation is comparable on different orientations including c -plane, a - and m -planes, as well as (10 $\bar{1}$ 3) and (11 $\bar{2}$ 2) planes^{18–20,22}. For MOVPE-grown InAlN, as aforementioned, comparable x_{InN} values have previously been found for c -plane vs. m -plane InAlN/GaN layers⁹, and c -plane vs. (11 $\bar{2}$ 2) InAlN/AlN layers²⁴. Additionally, comparable x_{InN} values have been found for N-polar and metal-polar c -plane InAlN/GaN⁵⁰. These results suggest that the impact of surface orientation on aluminium incorporation seems to be small or negligible for Al-containing alloys.

As aforementioned, growth parameters are very important for material incorporation. It is well-known that

TABLE I. In-plane strain state in a wurtzite crystal coordinate system with $x \parallel [11\bar{2}0]$, $z \parallel [0001]$, and $c' \parallel [30\bar{3}2]$ of the (0001), (10 $\bar{1}$ 3) and (10 $\bar{1}$ 0) InAlN/AlN layers grown on AlN templates at different growth temperatures.

Surface orientations		(0001)	(10 $\bar{1}$ 3)	(10 $\bar{1}$ 0)		
Materials	Growth temp. (°C)	ϵ_{xx} (10^{-4})	ϵ_{xx} (10^{-4})	$\epsilon_{c'}$ (10^{-4})	ϵ_{xx} (10^{-4})	ϵ_{zz} (10^{-4})
AlN	1290	7.8	-11.8	1.4	0.6	-1.8
	860	-40.5	-16.2	65.0	-1.6	7.4
InAlN	820	-76.2	-18.2	54.2	0.7	-3.1
	780	-65.3	-46.8	-20.2	-8.5	40.6
	740	-29.3	10.1	10.8	-4.5	22.4
	700	-30.1	47.4	-0.5	-13.7	59.8
	660	-39.8	21.7	-15.4	-13.6	58.4

parasitic reactions between TMGa, TmIn and NH_3 is much less severe than for TMAI and NH_3 ^{51,52}. Therefore, for Al-containing nitrides, suppressing these reactions is very essential to enhance growth efficiency and aluminium incorporation. Low growth pressures and low V/III ratios are generally used to grow AlGaIn^{3,14–16,18–20,22,51–53} and InAlN^{8,9,23,24}. It should be noted that low growth temperatures can also be used to reduce the reaction rate and gallium desorption, leading to an increased AlGaIn growth efficiency^{18,52,53}. For the InAlN layers studied here, the use of low temperatures, low pressure, and low V/III ratio suppressed the TMAI: NH_3 pre-reactions, resulting in the enhanced aluminium incorporation. Consequently, re-evaporation of InN volatile species can be suppressed, resulting in a higher indium incorporation. This also can explain why x_{InN} values of the grown c -plane, m -plane and (10 $\bar{1}$ 3) layers are comparable.

Tab. I shows the in-plane strain state of the differently oriented InAlN layers grown on AlN templates at different temperatures. Here, for example, the strain (ϵ_{xx}) along [11 $\bar{2}$ 0] was calculated as: $\epsilon_{xx} = (a_{\text{measurement}} - a_{\text{relax}}) / a_{\text{relax}}$. The strain ϵ_{zz} along [0001] (and $\epsilon_{c'}$ along [30 $\bar{3}$ 2] for the (10 $\bar{1}$ 3) layers) was calculated using the same manner. In Tab. I, it is clearly seen the anisotropic strain of the (10 $\bar{1}$ 3) and m -plane layers along two in-plane directions, e.g., $\epsilon_{xx} \neq \epsilon_{c'}$ obtained for the (10 $\bar{1}$ 3) layers and $\epsilon_{xx} \neq \epsilon_{zz}$ obtained for the m -plane layers.

B. Optical properties

1. Bandgap determination

To investigate optical bandgap of the grown layers, optical transmission measurements were performed at RT. From these measurements, Tauc plots⁵⁴ of $(\alpha h\nu)^2$ versus photon energy ($h\nu$) have been extracted to estimate absorption edge (i.e., effective energy bandgap E_g^{InAlN}) of the layers by extrapolating the linear portion from the plots, as shown in Fig. 3(a).

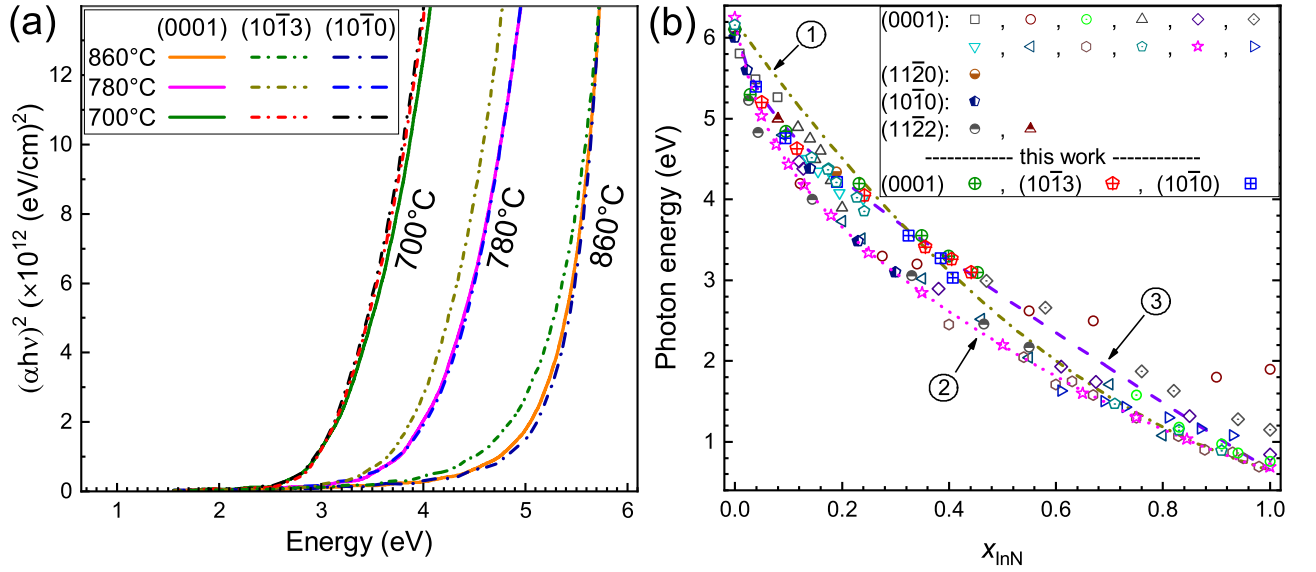


FIG. 3. (a) Tauc plots of the (0001), (10 $\bar{1}$ 3) and (10 $\bar{1}$ 0) InAlN co-loaded layers grown at three different temperatures. (b) Effective energy bandgap E_g of the grown layers [\oplus , \otimes , \oplus] plotted as a function of XRD-calculated x_{InN} . Bandgap data points previously reported for polar (0001) InAlN [\square ³⁷, \circ ³⁸, \odot ³⁹, \triangle ⁴⁰, \diamond ⁴¹, \diamond ⁴², ∇ ⁴³, \triangleleft ⁴⁴, \circ ⁴⁵, \diamond ⁴⁶, \star ⁴⁷, \triangleright ⁴⁸], nonpolar (11 $\bar{2}$ 0) InAlN [\bullet ³⁰] and (10 $\bar{1}$ 0) InAlN [\blacklozenge ⁹], as well as semipolar (11 $\bar{2}$ 2) InAlN [\bullet ²³, \blacktriangle ²⁴] are also plotted for comparison. The dash-dot line (1) is a fitting using Eq. 1 with b_x described in Eq. 2 [with $A \neq 0$ and $B = C = 0$]. The dot line (2) is a fitting to the data points (\star) reported in Ref. 47 using Eq. 1 [$A \neq 0$, $B \neq 0$, $C \neq 0$]. The dash line (3) is a fitting to the data points obtained in this study using Eq. 1 [$A \neq 0$, $B \neq 0$, $C \neq 0$].

E_g^{InAlN} values of the differently oriented layers are plotted as a function of XRD-calculated x_{InN} in Fig. 3(b). Their E_g^{InAlN} values are comparable, confirming their comparable x_{InN} . Fig. 3(b) also shows bandgap data previously reported for c -plane^{37–42,44–48}, a -plane³⁰, m -plane InAlN⁹, and (11 $\bar{2}$ 2) InAlN^{23,24}. It should be noted that almost these data points were estimated from RT optical measurements (e.g., transmission, reflectance and ellipsometry measurements), except data points of Wang *et al.*⁴³ and Schulz *et al.*⁴⁷ were estimated from low-temperature PL excitation measurements. Given the scattered data points in the literature, the E_g^{InAlN} values of the layers studied here are comparable^{24,30,40,42,43,46} or larger^{9,23,44,45,47}. This might be attributed to different characterization methods and different growth conditions. It should be noted that the effects of in-plane strain of our layers on the shift of E_g^{InAlN} can be neglected, as they only cause a shift of less than 0.05 eV estimated for the c -plane layers and less than 0.01 eV estimated for the m -plane and (10 $\bar{1}$ 3) layers. More important can be other effects of lateral decomposition due to grainy surface growth for relaxed and/or mismatched layers^{9,23,24}. This can lead to a low onset of adsorption in In-rich areas.

2. Bandgap bowing parameter

It is well-known that the effects of composition disorder on the conduction and valence band edges lead to a non-

linear behaviour of E_g of nitride alloys versus group-III composition⁵⁵. Therefore, a bandgap bowing parameter (b_x) is commonly used to determine this behaviour. This has previously reported for AlGa N ^{18,19,22,39,41} and InAl N ^{37–43,45–48}. For In $_x$ Al $_{1-x}$ N, the dependence of E_g^{InAlN} on x_{InN} is commonly described by the relation:

$$E_g^{\text{InAlN}} = x \cdot E_g^{\text{AlN}} + (1-x) \cdot E_g^{\text{InN}} - b_x \cdot x \cdot (1-x), \quad (1)$$

where

$$b_x = \frac{A}{1 + B \cdot x + C \cdot x^2}. \quad (2)$$

Here, A , B and C are adjustable parameters of the fit.

For InGa N ^{39,41} and AlGa N ^{18,19,22,39,41}, most groups do a fit with a composition-independent $b_x = b_0$, i.e., $A \neq 0$ and $B = C = 0$. This case has also been used to fit for InAlN layers^{37,40,45,48}. For the InAlN layers studied here, the shift of E_g^{InAlN} vs. x_{InN} can also be fitted using Eq. 1 with b_0 , which results in a bowing parameter of (4.0 ± 0.4) eV, as shown as the fitted line #1 in Fig. 3(b). For this fitting, values of $E_g^{\text{InN}} = 0.65$ eV¹ and $E_g^{\text{AlN}} = 6.2$ eV² have been fixed. Even though, this bowing value is in good agreement with values of about 4.0–5.0 eV previously reported for c -plane InAlN^{37,39,40,43,45,48}, this fitting does not satisfy the data points in the $x_{\text{InN}} < 0.2$ regime.

Compared to composition-independent fittings of InGaN ($b_0 \approx 1.4$ eV³⁹) and AlGaIn ($b_0 \approx 0.9$ - 1.0 eV^{18,19,22,39,41}), the bowing value of InAlN is much larger. Based on results obtained for InAlN layers with $x_{\text{InN}} \geq 0.4$, Jones *et al.*⁴⁵ have attributed this large value to band-filling effects, which might blue-shift the absorption edge of In-rich layers, and a stronger non-parabolic conduction band than valence band with decreasing x_{InN} .

Several groups have used a composition-dependent b_x to achieve a good fit of E_g^{InAlN} across investigated x_{InN} ^{41,44,46}. Two different cases [$A \neq 0, B \neq 0, C = 0$]^{41,44} and [$A \neq 0, B = 0, C \neq 0$]⁴⁶ have previously been used, which might be attributed to different E_g^{InAlN} achieved at those different groups. It has recently been reported that cation-related localized states strongly perturb the InAlN band structure, leading to a strong bandgap bowing at the low- x_{InN} regime^{47,56}. This has evidently been clarified by a combined experimental and theoretical study of E_g^{InAlN} across the entire range of x_{InN} of c -plane InAlN/GaN layers⁴⁷. Similar to the work of Jones *et al.*⁴⁵, a stronger non-parabolic conduction band than valence band has also been reported⁴⁷.

By fitting the data points of Schulz *et al.*⁴⁷ (\star in Fig. 3(b)) using Eqs. 1 and 2, we have found that using a case of [$A \neq 0, B \neq 0, C \neq 0$] gives the best fitting (the coefficient of determination R -squared = 0.9999), as shown as the fitted line #2 in Fig. 3(b). A , B , and C values are found to be (29.6 ± 0.1) eV, (12.5 ± 0.0) eV and (-5.0 ± 0.0) eV, respectively. (It should be noted that $E_g^{\text{InN}} = 0.65$ eV and $E_g^{\text{AlN}} = 6.2$ eV have also been fixed for this fitting). For the InAlN layers studied here, the shift of E_g^{InAlN} vs. x_{InN} can also be fitted using the same manner. Here, to compare with values obtained from the fitted line #2 and to achieve the best fitting, A and C values were fixed to be of 29.6 eV and -5.0 eV, respectively. This also results in the best fitting (R -squared = 0.9940) with a B value of (24.2 ± 0.9) eV, as shown as the fitted line #3 in Fig. 3(b).

3. Photoluminescence

For MOVPE-grown InAlN layers, a large Stokes-shift of up to 1 eV between bandgap energy and PL peak emission energy (E_{PL}) has previously been reported for c -plane⁴³, a -plane³⁰, m -plane⁹ and $(11\bar{2}2)$ layers²⁴ with $x_{\text{InN}} \leq 0.3$. This indicates large alloy fluctuations in those layers, which have been attributed to grainy morphology. This also somehow makes determination of InAlN near-band-edge (NBE) luminescence difficult if the NBE is close to impurity-related transitions of (Al,Ga)N underlayers^{9,57-61}.

For AlGaIn grown on sapphire, deep impurity transitions involving isolated cation vacancy with three-negative charges V_{III}^{3-} , cation vacancy complex with one-negative charges $(V_{\text{III}}\text{-complex})^{1-}$ (e.g., $(V_{\text{III}}\text{-O}_N)^{1-}$), and cation vacancy complex with two-negative charges

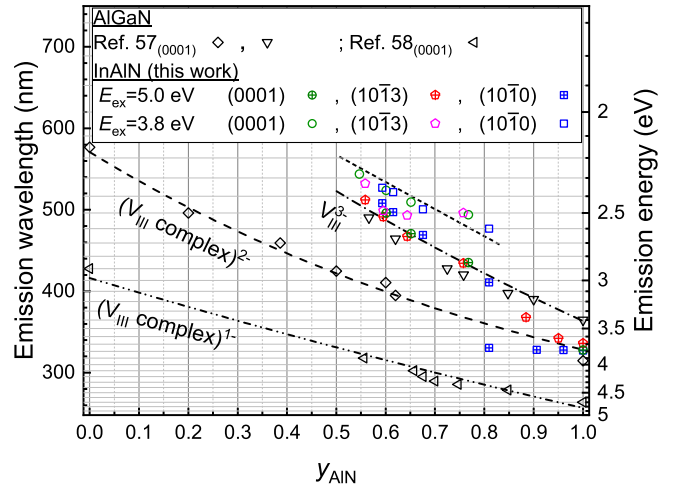


FIG. 4. RT-PL peak emission energy measured with the KrF excimer laser ($E_{\text{ex}} = 5.0$ eV) [\oplus , \oplus , \boxplus] and the He-Cd cw-laser ($E_{\text{ex}} = 3.8$ eV) [\circ , \diamond , \square] of the grown the (0001), $(10\bar{1}3)$ and $(10\bar{1}0)$ InAlN co-loaded layers plotted as a function of the AlN mole fraction ($y_{\text{AlN}} = 1 - x_{\text{InN}}$). RT-PL peak emission energies of V_{III}^{3-} and their complexes of c -plane AlGaIn layers reported in Refs. 57 and 58 are also plotted for comparison. Lines are guide to the eye.

$(V_{\text{III}}\text{-complex})^{2-}$ (e.g., $(V_{\text{III}}\text{-O}_N)^{2-}$) have previously been studied by RT-PL for layers with different surface orientations including c -plane^{16,57,58,62} and $(11\bar{2}2)$ ^{15,16}. The energy formation of cation vacancies and vacancy complexes has been found to follow the order⁵⁸: $V_{\text{III}}^{3-} < (V_{\text{III}}\text{-complex})^{2-} < (V_{\text{III}}\text{-complex})^{1-}$. Fig. 4 shows these impurity transitions obtained for c -plane AlGaIn plotted as a function of the AlN mole fraction (y_{AlN}). (Impurity transitions of $(11\bar{2}2)$ AlGaIn can be seen in Ref. 16.) It has been found that the formation of V_{III}^{3-} is more favourable in the $y_{\text{AlN}} \leq 0.5$ regime^{16,57}, while $(V_{\text{III}}\text{-complex})^{2-}$ can be formed in the whole range^{16,57}. Additionally, $(V_{\text{III}}\text{-complex})^{1-}$ has been found to form in the $y_{\text{AlN}} \geq 0.4$ regime^{16,58}.

Additionally, E_{PL} at around 3.6-3.8 eV of bulk AlN crystals has also been assigned to originate from substitutional carbon on nitrogen site (C_N)^{59,60}. A higher carbon concentration (e.g., $[\text{C}] \approx 2 \times 10^{17} \rightarrow 2 \times 10^{19} \text{ cm}^{-3}$) in AlN not only shifts the C_N -related E_{PL} to larger energy region but also lowers the E_{PL} intensity. The latter has been attributed to an insufficiency of carbon to act as the main acceptor⁵⁹. It has also been reported that a donor-acceptor-pair (DAP) involving C_N (e.g., $[\text{C}] \geq 10^{18} \text{ cm}^{-3}$) and nitrogen vacancy (V_N) corresponds to an E_{PL} at 2.8 eV⁶⁰. This DAP intensity was found to increase with increasing $[\text{C}]$.

For the grown InAlN layers here, RT-PL measurements were also performed ($E_{\text{ex}} = 5.0$ eV). Fig. 5 exemplifies PL spectra of the m -plane InAlN layers grown at different temperatures on m -plane AlN templates. (The c -plane and $(10\bar{1}3)$ co-loaded layers also have almost the same spectra, except the fact that the c -plane layers grown

at 660°C and 780-860°C do not emit light.) Spectra of the m -plane templates show only one UV band with an E_{PL} at about 3.8 eV and a full-width of half maximum (Δ_{PL}) of about 0.39 eV (after a Gaussian fitting of the corresponding band). For the layers grown at 780-860°C, their spectra also show an E_{PL} at almost the same position as obtained for the templates, irrespective of different x_{InN} ($\Delta_{\text{PL}} \approx 0.38$ -0.4 eV). This peak intensity decreases with decreasing InAlN growth temperature, e.g., a factor of nine between the layers grown at 860°C and 780°C (a factor of twelve compared with the AlN peak intensity). To compare with the impurity-related transitions obtained for AlGaIn, E_{PL} values of these investigated InAlN layers are also plotted as a function of $y_{\text{AlN}} = 1 - x_{\text{AlN}}$, as shown in Fig. 4. E_{PL} values of these layers do not nicely match the $(V_{\text{III-complex}})^{2-}$ line, thus this impurity transition can not be considered as the main cause. According to results previously reported for bulk AlN crystals⁵⁹, the dominant E_{PL} value at ~ 3.8 eV of the InAlN layers can be mainly attributed to the effects of C_{N} . This is plausible as $[C]$ should be higher in these layers grown at lower growth temperatures⁶³. This is a reason why the peak intensity of this C_{N} -related transition decreases with decreasing growth temperature. However, no DAP emission at 2.8 eV has been observed.

Besides the dominant UV band at 3.8 eV, the spectrum of the m -plane layer grown at 780°C also shows a very weak band (just above the noise level) with E_{PL} at about 3.0 eV. For the layers grown at below 780°C, the UV band completely disappears, instead of that, visible bands with $E_{\text{PL}} = 2.4$ -2.7 eV appear ($\Delta_{\text{PL}} \approx 0.3$ -0.5 eV). At lower growth temperatures, the O_{N} and C_{N} concentrations in the layers should be higher due to lower decomposition rates of NH_3 . This should lead to an appearance of O_{N} - and C_{N} -related transitions. However, E_{PL} values of the layers grown at 660-780°C only match the V_{III}^{3-} line.

Even though, for AlN layers grown by NH_3 -source molecular beam epitaxy (MBE)⁶⁴ it has been found that the density of V_{Al}^{3-} increases with decreasing growth temperature, MBE has completely different growth kinetics from MOVPE. A limited study on the effects of growth temperature at 1150°C and 1200°C on V_{Al}^{3-} -related defects in MOVPE-grown AlN layers has shown that the V_{Al}^{3-} concentration is lower at the lower temperature⁶⁵. Additionally, a previous study on the effects of relatively low growth temperatures at 540°C and 800°C on growth efficiency of MOVPE-grown AlN suggests that the lower temperature can reduce $\text{TMAI}:\text{NH}_3$ pre-reactions⁵³. Both these results are plausible due to the fact that the formation of the pre-reactions strongly depends on temperature⁵². Therefore, for the InAlN layers grown at 660-740°C studied here, we can exclude the effects of V_{III}^{3-} as the main cause for their E_{PL} values.

As visible E_{PL} vs. corresponding x_{InN} of the InAlN layers grown at 660-780°C closes their $E_{\text{g}}^{\text{InAlN}}$ vs. x_{InN} shown in Fig. 3(b), we attribute them to InAlN

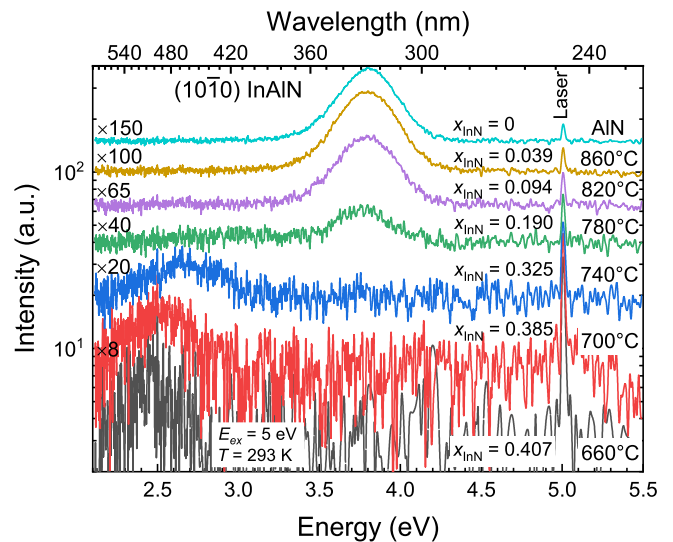


FIG. 5. RT-PL spectra measured with the KrF excimer laser ($E_{\text{ex}} = 5.0$ eV) of the m -plane InAlN layers grown at different temperatures on m -plane AlN templates.

NBE luminescence. The NBE peak intensity is weak, which might suggest that one state of the O_{N} - and C_{N} -related transitions still exists in the NBE. Due to the bandgap shrinking, these non-radiative channels become even stronger.

To confirm the InAlN NBE, RT-PL of these layers were also measured using the He-Cd laser ($E_{\text{ex}} = 3.8$ eV). (The layers grown at 820°C and 860°C do not emit light while being excited by this laser.) From their spectra (not shown), E_{PL} was also estimated using a Gaussian fitting ($\Delta_{\text{PL}} \approx 0.3$ -0.5 eV) and plotted in Fig. 4. This E_{PL} also decreases with decreasing y_{AlN} (increasing x_{InN}), however, it shifts about 0.1-0.2 eV to the lower energy region compared to the data points measured using the KrF laser. This is attributed to the stronger P_{ex} of the KrF laser than that of the He-Cd laser. A Stokes-shift of 0.6-0.9 eV has been estimated for these layers (based on E_{PL} using the KrF laser). This shift is comparable with values previously reported for differently oriented InAlN layers^{9,24,30,43}.

IV. CONCLUSIONS

MOVPE-growth of $\text{In}_x\text{Al}_{1-x}\text{N}$ layers ($0 \leq x_{\text{InN}} \leq 0.45$) simultaneously on polar (0001) AlN, untwinned semipolar (10 $\bar{1}$ 3) AlN and nonpolar (10 $\bar{1}$ 0) AlN templates was investigated. XRD-estimated x_{InN} values of all the co-loaded layers were found to be comparable. This is consistent with optical bandgap energy ($E_{\text{g}}^{\text{InAlN}}$) obtained from transmission measurements. An empirical relationship between $E_{\text{g}}^{\text{InAlN}}$ with x_{InN} was derived. The bandgap bowing parameter was found to be strongly composition-dependent. RT-PL measurements showed impurity transitions (e.g., $(V_{\text{III-O}_\text{N}})^{2-}$ and C_{N}) for the

layers with $x_{\text{InN}} \leq 0.2$, while InAlN NBE luminescence was observed for the layers with higher x_{InN} .

ACKNOWLEDGMENTS

The authors gratefully acknowledge the supports by the Program for Promoting the Enhancement of Research Universities. This work is also partially supported by Strategic International Collaborative Research Program (SICORP) of Japan Science and Technology Agency (JST), MOST-SKRDP (2016YFE0118400).

REFERENCES

- ¹C. S. Gallinat, G. Koblmüller, J. S. Brown, S. Bernardis, J. S. Speck, G. D. Chern, E. D. Readinger, H. Shen, M. Wraback, In-polar InN grown by plasma-assisted molecular beam epitaxy, *Appl. Phys. Lett.* 89 (3) (2006) 032109. doi:10.1063/1.2234274.
- ²H. Yamashita, K. Fukui, S. Misawa, S. Yoshida, Optical properties of AlN epitaxial thin films in the vacuum ultraviolet region, *J. Appl. Phys.* 50 (2) (1979) 896–898. doi:10.1063/1.326007.
- ³S. Keller, S. P. DenBaars, Metalorganic chemical vapor deposition of group III nitrides—a discussion of critical issues, *J. Cryst. Growth* 248 (2003) 479–486. doi:10.1016/S0022-0248(02)01867-5.
- ⁴D. F. Feezell, M. C. Schmidt, S. P. DenBaars, S. Nakamura, Development of nonpolar and semipolar InGa_xN/GaN visible light-emitting diodes, *MRS Bull.* 34 (5) (2009) 318–323. doi:10.1557/mrs2009.93.
- ⁵A. Laubsch, M. Sabathil, J. Baur, M. Peter, B. Hahn, High-power and high-efficiency InGa_xN-based light emitters, *IEEE Trans. Electron Devices* 57 (1) (2009) 79–87. doi:10.1109/TED.2009.2035538.
- ⁶M. Kneissl, T. Kolbe, C. Chua, V. Kueller, N. Lobo, J. Stellmach, A. Knauer, H. Rodriguez, S. Einfeldt, Z. Yang, N. M. Johnson, M. Weyers, Advances in group III-nitride-based deep UV light-emitting diode technology, *Semicond. Sci. Technol.* 26 (1) (2011) 014036. doi:10.1088/0268-1242/26/1/014036.
- ⁷H. Hirayama, Y. Enomoto, A. Kinoshita, A. Hirata, Y. Aoyagi, Room-temperature intense 320 nm band ultraviolet emission from quaternary InAlGa_xN-based multiple-quantum wells, *Appl. Phys. Lett.* 80 (9) (2002) 1589–1591. doi:10.1063/1.1456951.
- ⁸V. Z. Zubialevich, T. C. Sadler, D. V. Dinh, S. N. Alam, H. Li, P. Pampili, P. J. Parbrook, Enhanced UV luminescence from InAlN quantum well structures using two temperature growth, *J. Lumin.* 155 (2014) 108–111. doi:10.1016/j.jlumin.2014.06.033.
- ⁹S. F. Chichibu, K. Hazu, K. Furusawa, Y. Ishikawa, T. Onuma, T. Ohtomo, H. Ikeda, K. Fujito, High internal quantum efficiency ultraviolet to green luminescence peaks from pseudomorphic m-plane Al_xIn_{1-x}N epilayers grown on a low defect density m-plane freestanding GaN substrate, *J. Appl. Phys.* 116 (21) (2014) 213501. doi:10.1063/1.4902315.
- ¹⁰P. Pampili, V. Z. Zubialevich, P. Maaskant, M. Akhter, B. Corbett, P. J. Parbrook, InAlN-based LEDs emitting in the near-UV region, *Jpn. J. Appl. Phys.* 58 (SC) (2019) SCCB33. doi:10.7567/1347-4065/ab106b.
- ¹¹T. Takeuchi, S. Sota, M. Katsuragawa, M. Komori, H. Takeuchi, H. Amano, I. Akasaki, Quantum-confined Stark effect due to piezoelectric fields in GaInN strained quantum wells, *Jpn. J. Appl. Phys.* 36 (4A) (1997) L382. doi:10.1143/JJAP.36.L382.
- ¹²S. Takagi, Y. Enya, T. Kyono, M. Adachi, Y. Yoshizumi, T. Sumitomo, Y. Yamanaka, T. Kumano, S. Tokuyama, K. Sumiyoshi, N. Saga, M. Ueno, K. Katayama, T. Ikegami, T. Nakamura, K. Yanashima, H. Nakajima, K. Tasai, K. Naganuma, N. Fuutagawa, Y. Takiguchi, T. Hamaguchi, M. Ikeda, High-power (over 100 mW) green laser diodes on semipolar (20 $\bar{2}$ 1) GaN substrates operating at wavelengths beyond 530 nm, *Appl. Phys. Express* 5 (8) (2012) 082102. doi:10.1143/apex.5.082102.
- ¹³S. Ichikawa, Y. Iwata, M. Funato, S. Nagata, Y. Kawakami, High quality semipolar (1 $\bar{1}$ 02) AlGa_xN/AlN quantum wells with remarkably enhanced optical transition probabilities, *Appl. Phys. Lett.* 104 (25) (2014) 252102–1–4. doi:10.1063/1.4884897.
- ¹⁴J. Stellmach, F. Mehnke, M. Frentrop, C. Reich, J. Schlegel, M. Pristovsek, T. Wernicke, M. Kneissl, Structural and optical properties of semipolar (11 $\bar{2}$ 2) AlGa_xN grown on (10 $\bar{1}$ 0) sapphire by metal-organic vapor phase epitaxy, *J. Cryst. Growth* 367 (2013) 42–47. doi:10.1016/j.jcrysgro.2013.01.006.
- ¹⁵D. V. Dinh, S. N. Alam, P. J. Parbrook, Effect of V/III ratio on the growth of (11 $\bar{2}$ 2) AlGa_xN by metalorganic vapour phase epitaxy, *J. Cryst. Growth* 435 (2016) 12–18. doi:10.1016/j.jcrysgro.2015.11.009.
- ¹⁶D. V. Dinh, P. Pampili, P. J. Parbrook, Silicon doping of semipolar (11 $\bar{2}$ 2) Al_xGa_{1-x}N (0.50 ≤ x < 0.55), *J. Cryst. Growth* 451 (2016) 181–187. doi:10.1016/j.jcrysgro.2016.07.013.
- ¹⁷T. Wunderer, Z. Yang, M. Feneberg, M. Batres, M. Teepe, N. Johnson, Structural and optical characterization of Al-GaN multiple quantum wells grown on semipolar (20 $\bar{2}$ 1) bulk AlN substrate, *Appl. Phys. Lett.* 111 (11) (2017) 111101–1–3. doi:10.1063/1.4985156.
- ¹⁸D. V. Dinh, N. Hu, Y. Honda, H. Amano, M. Pristovsek, Aluminium incorporation in polar, semi-, and non-polar AlGa_xN layers: a comparative study of x-ray diffraction and optical properties, *Sci. Rep.* (accepted, Oct. 2019).
- ¹⁹D. V. Dinh, N. Hu, Y. Honda, H. Amano, M. M. Pristovsek, Untwinned semipolar (10 $\bar{1}$ 3) Al_xGa_{1-x}N layers grown on m-plane sapphire, *Semicond. Sci. Technol.* doi:10.1088/1361-6641/ab4d2c.
- ²⁰M. R. Laskar, T. Ganguli, A. A. Rahman, A. P. Shah, M. R. Gokhale, A. Bhattacharya, MOVPE growth and characterization of a-plane AlGa_xN over the entire composition range, *Phys. Status Solidi (RRL)* 4 (7) (2010) 163–165. doi:10.1002/pssr.201004091.
- ²¹M. Funato, K. Matsuda, R. G. Banal, R. Ishii, Y. Kawakami, Strong optical polarization in nonpolar (1 $\bar{1}$ 00) Al_xGa_{1-x}N/AlN quantum wells, *Phys. Rev. B* 87 (4) (2013) 041306. doi:10.1103/PhysRevB.87.041306.
- ²²D. V. Dinh, H. Amano, M. Pristovsek, Nonpolar m-plane Al_xGa_{1-x}N layers grown on m-plane sapphire by MOVPE, *J. Cryst. Growth* 512 (2019) 100–104. doi:10.1016/j.jcrysgro.2019.02.020.
- ²³N. Hatui, M. Frentrop, A. A. Rahman, A. Kadir, S. Subramanian, M. Kneissl, A. Bhattacharya, MOVPE growth of semipolar (11 $\bar{2}$ 2) In_xAl_{1-x}N across the alloy composition range (0 ≤ x ≤ 0.55), *J. Cryst. Growth* 411 (2015) 106–109. doi:10.1016/j.jcrysgro.2014.11.016.
- ²⁴D. V. Dinh, H. Li, P. J. Parbrook, Polar and semipolar (11 $\bar{2}$ 2) InAlN layers grown on AlN templates using MOVPE, *Phys. Status Solidi B* 253 (1) (2015) 99–104. doi:10.1002/pssb.201552264.
- ²⁵J. Stellmach, M. Frentrop, F. Mehnke, M. Pristovsek, T. Wernicke, M. Kneissl, MOVPE growth of semipolar (11 $\bar{2}$ 2) AlN on m-plane (10 $\bar{1}$ 0) sapphire, *J. Cryst. Growth* 355 (1) (2012) 59–62. doi:10.1016/j.jcrysgro.2012.06.047.
- ²⁶D. V. Dinh, H. Amano, M. Pristovsek, MOVPE growth and high-temperature annealing of (10 $\bar{1}$ 0) AlN layers on (10 $\bar{1}$ 0) sapphire, *J. Cryst. Growth* 502 (2018) 14–18. doi:10.1016/j.jcrysgro.2018.09.001.
- ²⁷M. Oseki, A. Kobayashi, J. Ohta, M. Oshima, H. Fujioka, Epitaxial growth of semipolar InAlN films on yttria-stabilized zirconia, *Phys. Status Solidi B* 254 (10) (2017) 1700211. doi:10.1002/pssb.201700211.
- ²⁸T. Kajima, A. Kobayashi, K. Ueno, K. Shimamoto, T. Fujii, J. Ohta, H. Fujioka, M. Oshima, Room-temperature epitaxial growth of high-quality m-plane InAlN films on nearly lattice-

- matched ZnO substrates, *Jpn. J. Appl. Phys.* 49 (7) (2010) 070202. doi:10.1143/jjap.49.070202.
- ²⁹T. Kajima, A. Kobayashi, K. Ueno, J. Ohta, H. Fujioka, M. Oshima, Structural properties of m-plane InAlN films grown on ZnO substrates with room-temperature GaN buffer layers, *Appl. Phys. Express* 6 (2) (2013) 021003. doi:10.7567/apex.6.021003.
- ³⁰M. R. Laskar, T. Ganguli, A. A. Rahman, A. Arora, N. Hattui, M. R. Gokhale, S. Ghosh, A. Bhattacharya, Anisotropic structural and optical properties of a-plane (11 $\bar{2}$ 0) AlInN nearly-lattice-matched to GaN, *Appl. Phys. Lett.* 98 (18) (2011) 181108. doi:10.1063/1.3583457.
- ³¹M. Hiroki, Y. Oda, N. Watanabe, N. Maeda, H. Yokoyama, K. Kumakura, H. Yamamoto, Unintentional Ga incorporation in metalorganic vapor phase epitaxy of In-containing III-nitride semiconductors, *J. Cryst. Growth* 382 (2013) 36–40. doi:10.1016/j.jcrysgro.2013.07.034.
- ³²S. Choi, H. J. Kim, Z. Lochner, J. Kim, R. D. Dupuis, A. M. Fischer, R. Juday, Y. Huang, T. Li, J. Y. Huang, F. A. Ponce, J.-H. Ryou, Origins of unintentional incorporation of gallium in AlInN layers during epitaxial growth, part I: Growth of AlInN on AlN and effects of prior coating, *J. Cryst. Growth* 388 (2014) 137–142. doi:10.1016/j.jcrysgro.2013.10.006.
- ³³J. Kim, Z. Lochner, M.-H. Ji, S. Choi, H. J. Kim, J. S. Kim, R. D. Dupuis, A. M. Fischer, R. Juday, Y. Huang, T. Li, J. Y. Huang, F. A. Ponce, J.-H. Ryou, Origins of unintentional incorporation of gallium in InAlN layers during epitaxial growth, part II: Effects of underlying layers and growth chamber conditions, *J. Cryst. Growth* 388 (2014) 143–149. doi:10.1016/j.jcrysgro.2013.09.046.
- ³⁴N. Hu, D. V. Dinh, M. Pristovsek, Y. Honda, H. Amano, How to obtain metal-polar untwinned high-quality (10 $\bar{1}$ 3) GaN on m-plane sapphire, *J. Cryst. Growth* 507 (2019) 205–208. doi:10.1016/j.jcrysgro.2018.11.013.
- ³⁵S. F. Chichibu, H. Yamaguchi, L. Zhao, M. Kubota, T. Onuma, K. Okamoto, H. Ohta, Improved characteristics and issues of m-plane InGaN films grown on low defect density m-plane freestanding GaN substrates by metalorganic vapor phase epitaxy, *Appl. Phys. Lett.* 93 (15) (2008) 151908. doi:10.1063/1.2998580.
- ³⁶H. Jönen, H. Bremers, U. Rossow, T. Langer, A. Kruse, L. Hoffmann, J. Thalmer, J. Zweck, S. Schwaiger, F. Scholz, A. Hangleiter, Analysis of indium incorporation in non- and semipolar GaInN QW structures: comparing x-ray diffraction and optical properties, *Semicond. Sci. Technol.* 27 (2) (2012) 024013. doi:10.1088/0268-1242/27/2/024013.
- ³⁷K. S. Kim, A. Saxler, P. Kung, M. Razeghi, K. Y. Lim, Determination of the band-gap energy of In_xAl_{1-x}N grown by metal-organic chemical-vapor deposition, *Appl. Phys. Lett.* 71 (6) (1997) 800–802. doi:10.1063/1.119650.
- ³⁸M. J. Lukitsch, Y. V. Danylyuk, V. M. Naik, C. Huang, G. W. Auner, L. Rimai, R. Naik, Optical and electrical properties of In_xAl_{1-x}N films grown by plasma source molecular-beam epitaxy, *Appl. Phys. Lett.* 79 (5) (2001) 632–634. doi:10.1063/1.1388883.
- ³⁹J. Wu, W. Walukiewicz, K. M. Yu, J. W. Ager, S. X. Li, E. E. Haller, H. Lu, W. J. Schaff, Universal bandgap bowing in group-III nitride alloys, *Solid State Commun.* 127 (6) (2003) 411–414. doi:10.1016/S0038-1098(03)00457-5.
- ⁴⁰R. Butté, E. Feltin, J. Dorsaz, G. Christmann, J.-F. Carlin, N. Grandjean, M. Illegems, Recent progress in the growth of highly reflective nitride-based distributed bragg reflectors and their use in microcavities, *Jpn. J. Appl. Phys.* 44 (10) (2005) 7207–7216. doi:10.1143/jjap.44.7207.
- ⁴¹M. Androulidaki, N. T. Pelekanos, K. Tsagaraki, E. Dimakis, E. Iliopoulos, A. Adikimenakis, E. Bellet-Amalric, D. Jalabert, A. Georgakilas, Energy gaps and bowing parameters of InAlGaN ternary and quaternary alloys, *Phys. Status Solidi C* 3 (6) (2006) 1866–1869. doi:10.1002/pssc.200565280.
- ⁴²H. Naoi, K. Fujiwara, S. Takado, M. Kurouchi, D. Muto, T. Araki, H. Na, Y. Nanishi, Growth of In-rich In_xAl_{1-x}N films on (0001) sapphire by RF-MBE and their properties, *J. Electron. Mater.* 36 (10) (2007) 1313–1319. doi:10.1007/s11664-007-0195-4.
- ⁴³K. Wang, R. W. Martin, D. Amabile, P. R. Edwards, S. Hernandez, E. Nogales, K. P. O'Donnell, K. Lorenz, E. Alves, V. Matias, A. Vantomme, D. Wolverson, I. M. Watson, Optical energies of AlInN epilayers, *J. Appl. Phys.* 103 (7) (2008) 073510. doi:10.1063/1.2898533.
- ⁴⁴E. Iliopoulos, A. Adikimenakis, C. Giesen, M. Heuken, A. Georgakilas, Energy bandgap bowing of InAlN alloys studied by spectroscopic ellipsometry, *Appl. Phys. Lett.* 92 (19) (2008) 191907. doi:10.1063/1.2921783.
- ⁴⁵R. E. Jones, R. Broesler, K. M. Yu, J. W. A. Iii, E. E. Haller, W. Walukiewicz, X. Chen, W. J. Schaff, Band gap bowing parameter of In_xAl_{1-x}N, *J. Appl. Phys.* 104 (12) (2008) 123501. doi:10.1063/1.3039509.
- ⁴⁶E. Sakalauskas, H. Behmenburg, C. Hums, P. Schley, G. Rossbach, C. Giesen, M. Heuken, H. Kalisch, R. H. Jansen, J. Bläsing, A. Dadgar, A. Krost, R. Goldhahn, Dielectric function and optical properties of Al-rich AlInN alloys pseudomorphically grown on GaN, *J. Phys. D: Appl. Phys.* 43 (36) (2010) 365102. doi:10.1088/0022-3727/43/36/365102.
- ⁴⁷S. Schulz, M. A. Caro, L.-T. Tan, P. J. Parbrook, R. W. Martin, E. P. O'Reilly, Composition-dependent band gap and band-edge bowing in AlInN: A combined theoretical and experimental study, *Appl. Phys. Express* 6 (12) (2013) 121001. doi:10.7567/APEX.6.121001.
- ⁴⁸R. C. Cramer, E. C. H. Kyle, J. S. Speck, Band gap bowing for high In-content InAlN films, *J. Appl. Phys.* 126 (3) (2019) 035703. doi:10.1063/1.5089671.
- ⁴⁹R. Bhat, G. M. Guryanov, Experimental study of the orientation dependence of indium incorporation in GaInN, *J. Cryst. Growth* 433 (2016) 7–12. doi:10.1016/j.jcrysgro.2015.09.022.
- ⁵⁰D. F. Brown, S. Keller, T. E. Mates, J. S. Speck, S. P. DenBaars, U. K. Mishra, Growth and characterization of In-polar and N-polar InAlN by metal organic chemical vapor deposition, *J. Appl. Phys.* 107 (3) (2010) 033509. doi:10.1063/1.3296127.
- ⁵¹C. H. Chen, H. Liu, D. Steigerwald, W. Imler, C. P. Kuo, M. G. Craford, M. Ludowise, S. Lester, J. Amano, A study of parasitic reactions between NH₃ and TMGa or TMAI, *J. Electron. Mater.* 25 (6) (1996) 1004–1008. doi:10.1007/BF02666736.
- ⁵²T. G. Mihopoulos, V. Gupta, K. F. Jensen, A reaction-transport model for AlGaIn MOVPE growth, *J. Cryst. Growth* 195 (1) (1998) 733–739. doi:10.1016/S0022-0248(98)00649-6.
- ⁵³D. G. Zhao, J. J. Zhu, D. S. Jiang, H. Yang, J. W. Liang, X. Y. Li, H. M. Gong, Parasitic reaction and its effect on the growth rate of AlN by metalorganic chemical vapor deposition, *J. Cryst. Growth* 289 (1) (2006) 72–75. doi:10.1016/j.jcrysgro.2005.11.083.
- ⁵⁴J. Tauc, R. Grigorovici, A. Vancu, Optical properties and electronic structure of amorphous germanium, *Phys. Status Solidi B* 15 (2) (1966) 627–637. doi:10.1002/pssb.19660150224.
- ⁵⁵J. A. Van Vechten, T. K. Bergstresser, Electronic structures of semiconductor alloys, *Phys. Rev. B* 1 (1970) 3351–3358. doi:10.1103/PhysRevB.1.3351.
- ⁵⁶S. Schulz, M. A. Caro, E. P. O'Reilly, Impact of cation-based localized electronic states on the conduction and valence band structure of Al_xIn_{1-x}N alloys, *Appl. Phys. Lett.* 104 (17) (2014) 172102. doi:10.1063/1.4872317.
- ⁵⁷K. B. Nam, M. L. Nakarmi, J. Y. Lin, H. X. Jiang, Deep impurity transitions involving cation vacancies and complexes in AlGaIn alloys, *Appl. Phys. Lett.* 86 (22) (2005) 222108. doi:10.1063/1.1943489.
- ⁵⁸N. Nepal, M. L. Nakarmi, J. Y. Lin, H. X. Jiang, Photoluminescence studies of impurity transitions in AlGaIn alloys, *Appl. Phys. Lett.* 89 (9) (2006) 092107. doi:10.1063/1.2337856.
- ⁵⁹R. Collazo, J. Xie, B. E. Gaddy, Z. Bryan, R. Kirste, M. Hoffmann, R. Dalmau, B. Moody, Y. Kumagai, T. Nagashima, Y. Kubota, T. Kinoshita, A. Koukitsu, D. L. Irving, Z. Sitar, On the origin of the 265 nm absorption band in AlN bulk crystals, *Appl. Phys. Lett.* 100 (19) (2012) 191914–1–5.

- [doi:10.1063/1.4717623](https://doi.org/10.1063/1.4717623).
- ⁶⁰B. E. Gaddy, Z. Bryan, I. Bryan, R. Kirste, J. Xie, R. Dalmau, B. Moody, Y. Kumagai, T. Nagashima, Y. Kubota, T. Kinoshita, A. Koukitu, Z. Sitar, R. Collazo, D. L. Irving, Vacancy compensation and related donor-acceptor pair recombination in bulk AlN, *Appl. Phys. Lett.* 103 (16) (2013) 161901. [doi:10.1063/1.4824731](https://doi.org/10.1063/1.4824731).
- ⁶¹T. Koppe, H. Hofsäss, U. Vetter, Overview of band-edge and defect related luminescence in aluminum nitride, *J. Lumin.* 178 (2016) 267–281. [doi:10.1016/j.jlumin.2016.05.055](https://doi.org/10.1016/j.jlumin.2016.05.055).
- ⁶²Q. Yan, A. Janotti, M. Scheffler, C. G. Van de Walle, Origins of optical absorption and emission lines in AlN, *Appl. Phys. Lett.* 105 (11) (2014) 111104. [doi:10.1063/1.4895786](https://doi.org/10.1063/1.4895786).
- ⁶³J.-T. Chen, U. Forsberg, E. Janzén, Impact of residual carbon on two-dimensional electron gas properties in $\text{Al}_x\text{Ga}_{1-x}\text{N}/\text{GaN}$ heterostructure, *Appl. Phys. Lett.* 102 (19) (2013) 193506. [doi:10.1063/1.4804600](https://doi.org/10.1063/1.4804600).
- ⁶⁴T. Koyama, M. Sugawara, T. Hoshi, A. Uedono, J. F. Kaeding, R. Sharma, S. Nakamura, S. F. Chichibu, Relation between Al vacancies and deep emission bands in AlN epitaxial films grown by NH_3 -source molecular beam epitaxy, *Appl. Phys. Lett.* 90 (24) (2007) 241914. [doi:10.1063/1.2748315](https://doi.org/10.1063/1.2748315).
- ⁶⁵J.-M. Mäki, F. Tuomisto, B. Bastek, F. Bertam, J. Christen, A. Dadgar, A. Krost, Effect of growth conditions on vacancy defects in MOVPE grown AlN thin layers, *Phys. Status solidi C* 6 (11) (2009) 2575–2577. [doi:10.1002/pssc.200982108](https://doi.org/10.1002/pssc.200982108).